ACS OMEGA

Open Access

http://pubs.acs.org/journal/acsodf

Article

Transfer of AuNRs into AAO Nanoholes via Self-Assembly Method for Ultrasensitive SERS Detection

Ziqing Fang, Jun Dong,* Yimeng Fan, Chenlu Li, Qingyan Han, Chengyun Zhang, Lipeng Zhu, Xuewen Yan, Jianxia Qi, and Wei Gao*

Cite This: *ACS Omega* 2025, 10, 18764−18774

Read Online

ACCESS | Metrics & More | Article Recommendations | Supporting Information

ABSTRACT: Surface-enhanced Raman scattering (SERS) has become an advanced spectroscopic analysis method in the fields of chemistry, biomedical sensing, and imaging, owing to its excellent vibrational signal recognition and sensitivity for single-molecule detection. The effectiveness of SERS technology relies on the development of high-performance substrates, which must possess high sensitivity, uniformity, and repeatability. In this study, the enhanced substrates with high Raman activity were successfully prepared by adopting the three-phase self-assembly method to assemble gold nanorods (AuNRs) into nanopores of ultrathin porous alumina (AAO) films. By precisely controlling the pore size of AAO and the dimensions of AuNRs, the ability of the substrates and the Raman detection limits are enhanced significantly. Probe molecules, including Rhodamine 6G (R6G), Crystal Violet (CV), and Aspartame (APM), were selected to test the substrates sensitivity and uniformity, with detection limits of 10^{-13}, 10^{-12} M, and 7.8 mg/L, respectively. Random sampling was conducted on the substrate surface to analyze the spectral characteristics of the characteristic peaks of R6G and CV molecules, and the relative standard deviations (RSD) were 4.3 and 3.18% at characteristic peaks 612 and 1619 cm^{-1}, respectively, demonstrating the enhanced uniformity of the prepared substrates. This research indicates that assembling AuNRs onto AAO substrates results in significant Raman activity, providing a more reliable platform for the application of SERS technology.

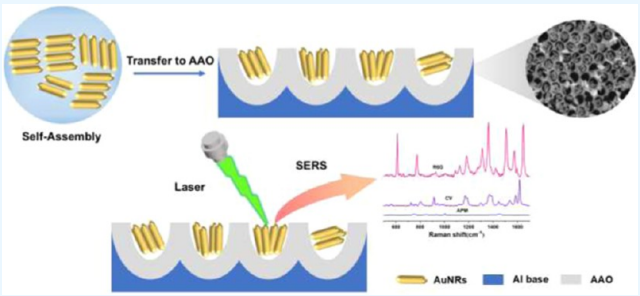

1. INTRODUCTION

Surface-enhanced Raman scattering (SERS) is a spectroscopic technique that can significantly amplify the Raman scattering signals of analyte molecules on rough metal surfaces, achieving signal enhancements of up to millions of times.[1−3] Due to its highly sensitive vibrational fingerprint information and single-molecule detection capability in biomedical and chemical sensing, SERS has emerged as an ideal platform for rapid, nondestructive testing.[4−10] Consequently, the fabrication of high-performance SERS substrates has attracted increasing interest from researchers.[11] Under specific excitation conditions, noble metal nanostructures exhibit unique surface plasmon resonance (SPR) effects, which can significantly enhance the local electromagnetic field. Nevertheless, numerous deficiencies exist in disordered nanostructures. These deficiencies can not only disrupt the optical response but also lead to poor repeatability and a lack of controllability. In contrast, when nanostructures possess periodic characteristics, they will exhibit special surface plasmon resonance properties, which are capable of generating a uniform and orderly enhancement of the local electric field on the surface of the nanostructures. This enhanced effect is particularly important for spectroscopic techniques such as SERS, as it can significantly increase the intensity of spectral signals, thereby improving detection limits for molecules and achieving good reproducibility. Therefore, further research on the development of periodically ordered SERS substrates is of great significance in the field of SERS detection.

Local electromagnetic enhancement based on resonance coupling effects can be achieved by varying the size, spacing and periodicity of nanoparticles.[12−15] Currently, methods for preparing periodically ordered noble metal micro- and nanostructures include ion beam etching, photolithography, nanoimprinting, and template methods. These approaches can yield SERS substrates with well-defined morphologies and uniform sizes, such as nanopillar arrays,[16,17] grating arrays,[18,19] and nanoparticle arrays.[20,21] Among these, the template method has become a particularly attractive approach for synthesizing nanostructures and nanostructured arrays in recent years. Template-based methods can produce nanostructures with very clear high aspect ratios. Compared to traditional manufacturing techniques such as photolithography or ion

Received: January 14, 2025
Revised: April 8, 2025
Accepted: April 28, 2025
Published: May 2, 2025

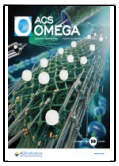

https://doi.org/10.1021/acsomega.5c00417
ACS Omega 2025, 10, 18764−18774

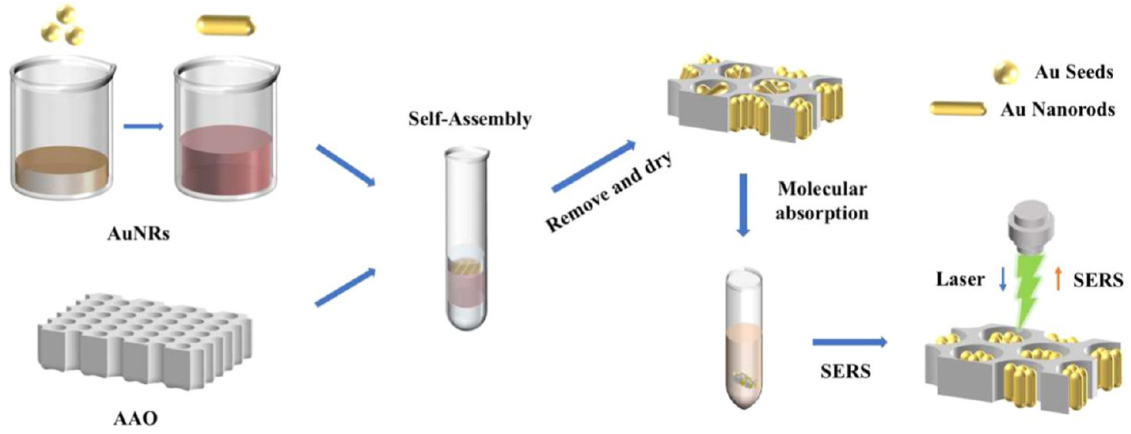

Figure 1. Schematic diagram of the fabrication of AuNR@AAO SERS substrate.

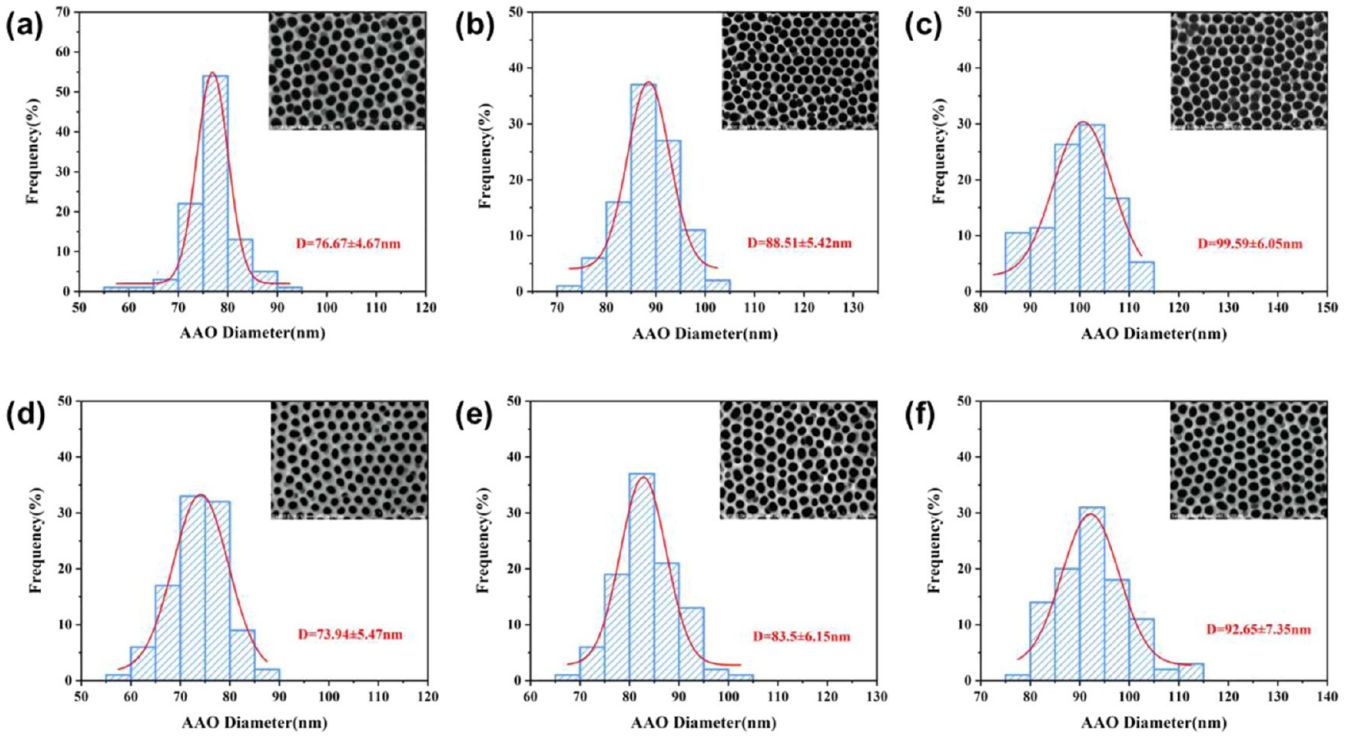

Figure 2. Histograms of the pore size distribution of AAO under different oxidation voltages and the pore expansion times based on SEM characterization images. (a) 45 V, 40 min; (b) 45 V, 45 min; (c) 45 V, 50 min; (d) 50 V, 40 min; (e) 50 V, 45 min; (f) 50 V, 50 min.

etching, this method is cost-effective, easy to operate, widely applicable, and capable of achieving nanoscale precision,[22,23] making it suitable for large-scale production and application promotion. Among them, anodic aluminum oxide (AAO) is the most commonly used template. Whether as a porous material itself or as a template for fabricating various nanostructures, AAO demonstrates excellent adaptability as a platform for numerous applications.[24] It has flexible and controllable dimensions, outstanding pore uniformity, and uniformly arranged porosity, exhibiting significant long-range ordered characteristics. Additionally, AAO templates have high temperature resistance, good insulation properties, and excellent stability, making them widely used in the preparation and study of low-dimensional nanostructural materials, such as synthesized nanofibers, nanotubes,[25] and nanoparticle arrays.

Gold nanorods (AuNRs) with unique optical properties are widely used in SERS-related applications.[26,27] In order to assemble precious metal nanoparticles such as nanorods into the gaps of nanostructured templates, previous researchers used AAO as a template and adopted, electrochemical deposition[28,29] and ultrasonic[30−32] methods to prepare AuNRs array substrates and realize SERS applications. In particular, Wang et al.[33] realized the restricted assembly of polystyrene-tethered AuNRs (AuNRs@PS) with different morphologies in the channels of two-pass AAO by external electric field assistance. However, the template-assisted substrate preparation methods mentioned above have high requirements and limitations in terms of technology and experimental equipment. Therefore, it is necessary to develop low-cost, reproducible and facile methods to produce SERS substrates. Song et al.[34] overcame the limitations of traditional methods by employing an assembly strategy based on interfacial interactions. They utilized the pore confinement effect of ultrathin AAO templates and regulated intermolecular forces to achieve an ultradense and orderly

https://doi.org/10.1021/acsomega.5c00417
ACS Omega 2025, 10, 18764−18774

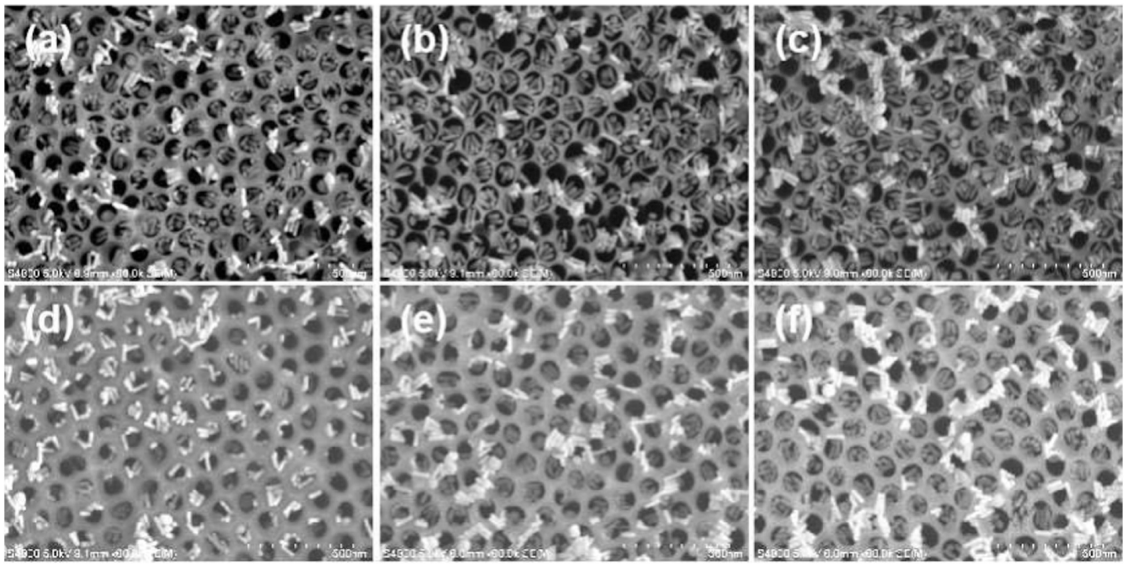

Figure 3. (a−c) Oxidation voltage was 45 V, and the pore expansion time was 40, 45, and 50 min, respectively. (d−f) The oxidation voltage was 50 V, and the pore expansion time was 40, 45, and 50 min, respectively.

arrangement of gold nanoparticles. This approach simplified the preparation process while significantly enhancing the sensitivity and repeatability of SERS substrates. Their work demonstrates that the coordinated optimization of interface engineering and template methods is a crucial direction for developing low-cost, high-performance SERS substrates.

In this paper, highly efficient and ordered SERS detection substrates are prepared by a simple and low-cost method, based on the template method and the three-phase self-assembly technique. The experimental results show that the AAO pore size as well as pore depth, and the size of the AuNRs all have a certain effect on the enhancement effect of the substrate. It should be noted that the three-phase interfacial self-assembly technique, highly reproducible and homogeneous nanoparticle monolayers can be prepared, but the technique does not result in the directional alignment of the particles. The substrate has high SERS activity, and exhibits detection limits of 1.0×10^{-13}, 1.0×10^{-12} M, and 7.8 mg/L for R6G, CV, and APM probe molecules. Moreover, the substrates are highly reproducible and homogeneous, with high value and potential for engineering applications.

2. RESULTS AND DISCUSSION

The periodic arrangement of AuNR arrays can be accomplished by precisely controlling the preparation conditions of AAO templates and the deposition process of the AuNRs. This nanostructure not only displays a highly ordered arrangement but also reveals distinct geometric shapes at the nanoscale, which offers a controllable approach for in-depth research on the properties of nanomaterials and their potential applications.

2.1. Preparation and Characterization of AuNRs@AAO Substrates. The preparation of AuNRs@AAO substrates strongly depends on factors, such as temperature, voltage, and the concentration of colloidal solutions. The schematic synthesis of this substrate is shown in Figure 1. First, according to previous researches, it is known that anisotropic nanoparticles have richer scattering properties than spherical nanoparticles.[35,36] AuNRs possess this characteristic. To achieve significant electromagnetic enhancement signals, it is essential to design and synthesize nanoparticles. By adjusting the aspect ratio of the nanorods, the position and intensity of their absorption spectra can be changed enabling them to selectively absorb and scatter light of different wavelengths. Therefore, in this study, we first synthesized AuNR colloids with different aspect ratios. Second, in order to assemble AuNRs into the AAO pores, appropriate AAO templates need to be prepared. Specifically, an ultrathin AAO template with different pore diameters was prepared by adjusting experimental conditions such as the oxidation voltage of the AAO, secondary oxidation time, and pore widening time. The preparation procedure of the AAO template is described in the Supporting Information. The relationship between parameters such as the oxidation voltage, expansion time and the pore size of the generated AAO template is detailed in Figure 2. Figure S1 shows the vertical section of the naturally fractured AAO film and measures the average hole depth to be about 88 nm.

During the synthesis of AuNRs, hexadecyltrimethylammonium bromide (CTAB), an amphiphilic molecule, presents challenges for direct assembly at the oil/water interface. Consequently, a self-assembly process of CTAB-stabilized nanoparticles is required to achieve ligand exchange from CTA^+ to poly(vinylpyrrolidone) (PVP), resulting in the preparation of PVP-coated AuNRs. During the assembly process, on the one hand, PVP forms a protective layer on the surface of the nanorods through its hydrophobic chains. This effectively prevents the nanorods from aggregating in the ethanol solution and maintains their uniform dispersion by means of the steric hindrance effect. On the other hand, the PVP-coated gold nanorods can easily form a dense monolayer film at the oil/water interface. Moreover, they can facilitate the transfer of gold nanorods from the lower oil−water interface to the upper oil−water interface. To assemble the AuNRs into AAO pores, we developed a highly reproducible gold nanoparticle membrane using a three-phase oil/water/oil system based on the Marangoni effect. The optical characterization of the three-phase assembled AuNR film is detailed in Figure S2b. The preparation process consists of four steps: (1) PVP-coated AuNRs were added to a mixture of dichloromethane and absolute ethanol. (2) After a short period of rapid mechanical shaking, the nanoparticles were transferred to the water-

https://doi.org/10.1021/acsomega.5c00417
ACS Omega 2025, 10, 18764−18774

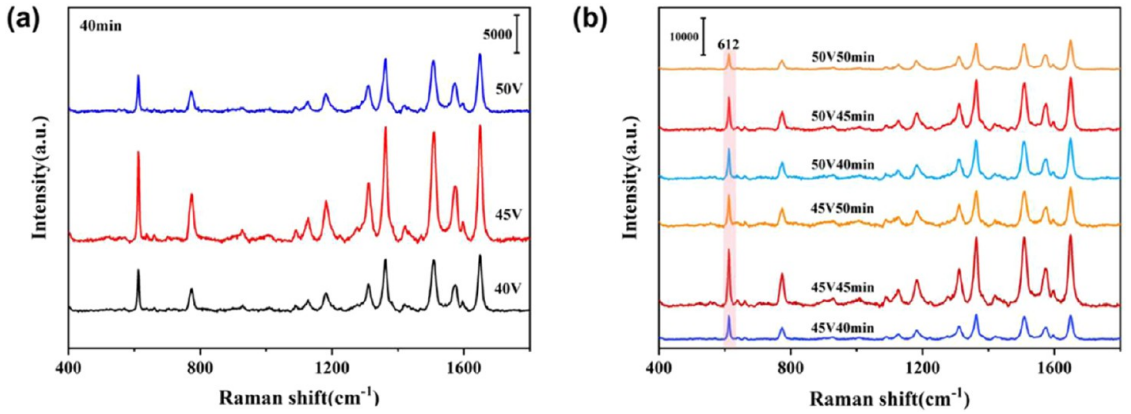

Figure 4. (a) Comparison diagram of R6G Raman spectrum of substrate adsorption under different oxidation voltage when the pore expansion time is 40 min; (b) Raman spectrum of the substrate at R6G of 10^{-6} M for different oxidation voltages and expansion time.

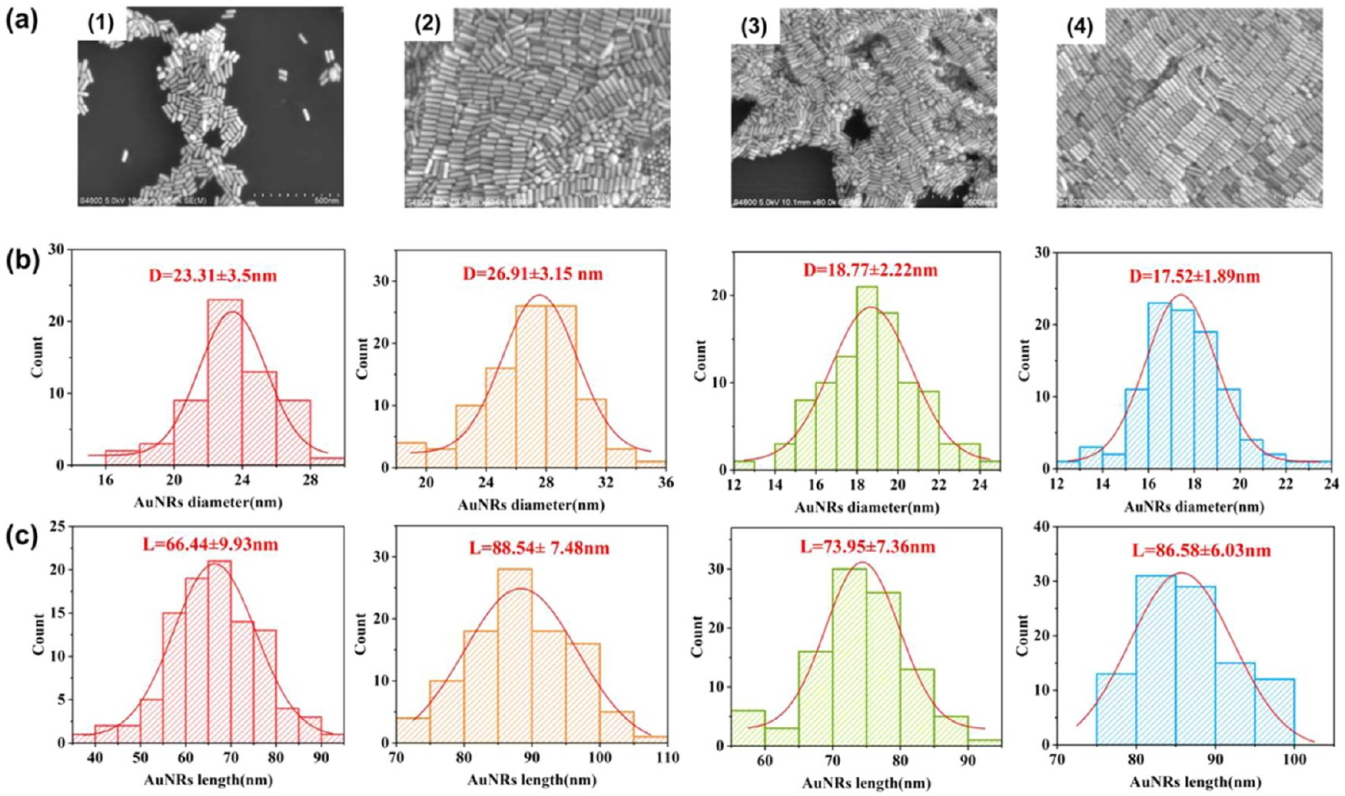

Figure 5. (a) From left to right, the SEM images of 714, 800, 813, and 880 nm AuNRs taken after being naturally dropped onto a silicon wafer and dried. Statistical graph of the diameter (b) and length (c) of AuNRs with different aspect ratios.

dichloromethane interface, forming a gold film layer. (3) After the addition of *n*-hexane, the nanoparticles rapidly migrated to the water-*n*-hexane interface. (4) A needle tube was used to remove *n*-hexane, and single-layer nanoparticles were transferred to the surface of AAO substrate. In preparation, the nanoparticles were transferred and aggregated due to the action of Marangoni force, which arose from the gradient difference in surface tension between the two interfaces. When the surface tension at the upper water/oil interface is greater than that at the lower oil/water interface, the Marangoni force overcomes the electrostatic repulsion between the nanoparticles, and pulls them upward to form a highly reproducible monolayer film.[37] The monolayer films prepared using the three-phase assembly method exhibited no clustering, providing a solid foundation for the uniform SERS substrate (see in Figure S2c).

AAO films prepared under varying experimental conditions are shown in Figure 2. Additionally, the AuNR particles were assembled into AAO with different pore sizes by the three-phase assembly method, and periodically distributed AuNR arrays were fabricated as depicted in Figure 3. The scanning electron microscopy (SEM) characterization confirms that the filling rate of the AAO pores is almost 100%.

The effective entry of AuNRs into the AAO pores is attributed to the synergistic effect of several critical factors. First, the matching of AuNRs size and AAO aperture largely ensures that the particles can enter the pore smoothly. Second, the capillary force of the AAO pore induces the AuNRs to move along the pore wall and fill the pore. The nanopore must be completely wetted by the nanocolloid to successfully assemble the nanoparticles into the nanopore.[38] Although the concentration

https://doi.org/10.1021/acsomega.5c00417
ACS Omega 2025, 10, 18764−18774

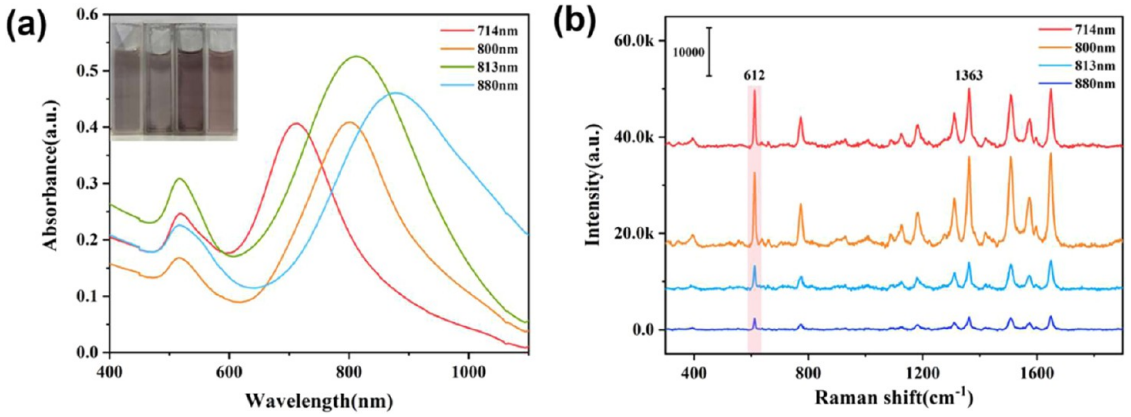

Figure 6. (a) UV absorption spectra of AuNRs at different LSPR position. The upper left corner is the color comparison diagram of AuNRs (200 μL) diluted with deionized water. (b) Comparison graph of Raman signal intensity of AuNRs with different aspect ratios assembled into AAO.

and transfer rate of the nanorods may have some impact on their ordered arrangement in the pores, the films formed by the three phases interface are able to infiltrate the nanopores, which contributes to the uniform distribution and deposition of the nanoparticles. Finally, the pore of Al_2O_3 material is hydrophilic, together with the porous structure and ultrathin thickness of AAO, which not only increases the contact area with water molecules, but also provides an ideal template for the AuNRs with its highly ordered structure. It induces the particles to form an ordered structure, and improves the filling efficiency and uniformity of the template. The combined effect of the above factors can enable the AuNR particles to enter the AAO and form relatively ordered nanostructures.

Figure 3a–f show that the majority of AuNRs enter the nanopores of the AAO substrate, while a small amount of AuNR clusters remain outside the pores. This phenomenon could be attributed to the following reasons. First, the limited pore size and shape of the AAO restrict the entry of AuNRs, with smaller pores preventing larger particles from entering. And partially filled AAO pores hinder the entry of subsequently added particles. Second, uneven distribution of capillary force leads to nonuniform adsorption or arrangement of particles within the holes. Third, according to Redon et al.,[39,40] the surface tension of water is strong enough to overcome the attraction between AAO and water. As a result, the nanoparticles tend to stick together. Moreover, the particle surfaces are hydrophilic, which makes particles easier for them to aggregate with each other to form stable cluster structures instead of entering the nanopores. The dynamics of the self-assembly process, including the deposition rate of the particles and the evaporation rate of the solvent, also affect the distribution of gold nanorods in the AAO pores.[41] In this regard, some measures have been taken, including adjusting the concentration of gold nanorods colloidal solution (as shown in Figure S2a), using filter paper to adsorb excess nanoparticles timely and rinsing the sample surface with deionized water, which has reduced the number of external cluster particles outside the pores to some extent.

The SERS activity of the substrate was investigated under different pore size conditions. As illustrated in Figure 3, when the oxidation voltage increases, the pore size of AAO becomes larger with the subsequent increase in the number of AuNRs filled in the pore. The substrate was immersed in a solution of R6G molecules at a concentration of 10^{-6} M and Raman spectra were acquired as shown in Figure 4. First, the pore expansion time was set to 40 min, and the oxidation voltage value was adjusted. The Raman spectrum was collected, as shown in Figure 4a. It is evident that the substrate exhibited the strongest Raman activity with AAO prepared at an oxidation voltage of 45 V. Second, the oxidation voltage was adjusted to the optimal value of 45 V, and the SERS enhancement effect with different pore expansion times was analyzed. As demonstrated in Figure 4b, the strongest Raman signals of the probe molecules were obtained when the oxidation voltage was set to 45 V and the expansion time was 45 min.

It is well-known that the aspect ratio of AuNRs also has an effect on the substrate enhancement effect. The AuNRs of 714, 800, 813, and 880 nm were selected for exploration. Figure 5a shows the SEM image of AuNRs, measuring the length and diameter of AuNRs respectively, and drawing the frequency histograms, the results are presented in Figure 5b,c. The aspect ratio of AuNRs for different LSPR peaks is 714 nm gold rod is about 2.85, 800 nm gold bar is about 3.29, 3.94 for 813 nm, and 880 nm gold rod is about 4.92. The LSPR peaks are gradually red-shifted with increasing aspect ratio.

The UV-vis absorption spectra of four AuNRs with different localized surface plasmon resonances (LSPRs) are presented in Figure 6a, which shows that the absorbance peak of the AuNRs is red-shifted and the color of the colloid is slowly transformed from violet to red with the increase of LSPR wavelength. Figure 6b shows the Raman spectrum of a 10^{-6} M R6G molecular solution adsorbed onto a substrate with different AuNRs, where the LSPR wavelengths of the AuNRs used to assemble the substrate are consistent with the four distinct LSPR wavelengths shown in Figure 6a. It is evident that when the LSPR of the AuNR is at 800 nm, the assembled substrate exhibits the best Raman enhancement effect. The Raman intensity of the substrate shows an initial increase followed by a decrease with the size of the AuNRs, rather than exhibiting a continuous increase. It is noteworthy that the length of the AuNRs with the LSPR peak of 880 nm (with an average length of 88 nm, as shown in Figure 5c) precisely matched the pore depth of the AAO template with a pore expansion time of 2 min (around 88 nm). This geometric compatibility not only facilitated the vertical alignment of AuNRs within the AAO channels but also effectively mitigated issues such as significant tilting caused by insufficient length or clustering outside the pores due to excessive length. More importantly, the nanorod tips generate localized electromagnetic field enhancement through the tip effect, while the sub-10 nm gaps between adjacent AuNRs create high-density plasmonic "hot spots". This dual enhancement

https://doi.org/10.1021/acsomega.5c00417
ACS Omega 2025, 10, 18764−18774

mechanism further optimizes the uniformity of electromagnetic field distribution and molecular adsorption sites. Consequently, the optimal experimental conditions are an oxidation voltage of 45 V, a pore expansion time of 45 min, and an LSPR of 800 nm for AuNRs. The prepared sample under the conditions will be used for subsequent research.

2.2. SERS Activity of AuNRs@AAO Substrate. The SERS performance of the bare AAO, pure AuNRs arrays, and AuNRs@AAO substrate was compared using 10^{-6} M R6G as the probe molecule. As shown in Figure 7, the AuNRs@AAO

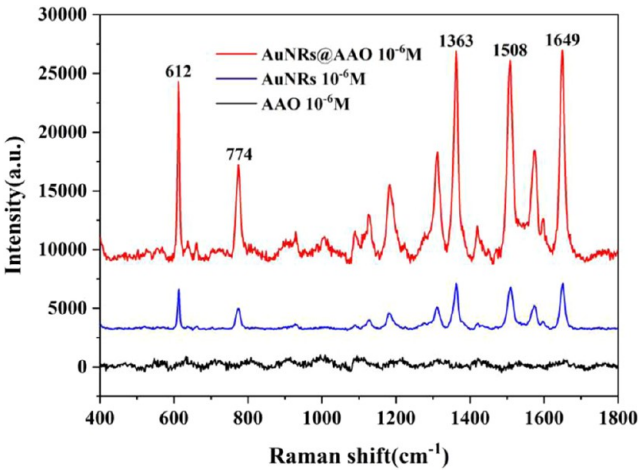

Figure 7. Comparison of Raman spectra for bare AAO, pure AuNRs array, and AuNRs@AAO substrate adsorbed with 10^{-6} M R6G under identical experimental conditions.

substrate exhibited significantly higher Raman intensity than the other two substrates, with characteristic peaks of R6G clearly observed, such as 612, 774, and 1363 cm^{-1}. This remarkable SERS enhancement effect is attributed to the unique nanostructure of the AuNRs@AAO substrate and its high-density plasmonic hot spots. In contrast, the bare AAO substrate showed negligible Raman signals, while the pure AuNRs arrays fabricated by three-phase self-assembly on a silicon wafer demonstrated moderate enhancement due to the lack of ordered nanostructure.

In order to effectively evaluate the performance of substrate-enhanced Raman scattering, R6G molecules were used as detection targets for Raman spectroscopy testing. The AuNRs@AAO substrate was immersed in R6G solution for 60 min then removed and left to dry naturally. The blank samples are AAO without assembling particles, absorbing R6G molecule with a concentration of 10^{-3} M, and the Raman spectra are shown in Figure S3a. It can be seen that AAO itself weakly enhanced the Raman signal of R6G molecule at this concentration. Figure 8a shows that Raman spectra of R6G molecules on the AuNRs@AAO substrate under laser excitation at a wavelength of 532 nm. It can be seen clearly that the Raman signal of the probe is effectively enhanced, and the substrate can achieve the detection of R6G molecules with a concentration of 10^{-13} M. Figure 8b displays the amplified Raman spectra for R6G concentrations of 10^{-12} and 10^{-13} M in Figure 8a. The laser excitation power was set to 2.5 mW, with an integration time of 5 s. In the range of 500 to 1700 cm^{-1}, the characteristic Raman peaks of R6G are distinctly observed at 612, 774, 1182, 1311, 1361, 1509, and 1649 cm^{-1}, which approximately coincide with the previous report.[42]

The detection limit of the substrate was studied. As the concentration decreased, the Raman signal of R6G gradually weakened. When the concentration of R6G was reduced to 10^{-13} M, Raman peaks at 614, 1364, 1508, and 1648 cm^{-1} could still be observed. The limit of detection (LOD) was further calculated based on the calibration curve, with detailed methods and results provided in the Supporting Information (Detection Limits of AuNRs@AAO Substrates). The AAO substrate assembled with AuNRs exhibits strong Raman activity.[43] The localized electromagnetic field enhancement at the gaps between adjacent nanorods can effectively increase the Raman scattering signal intensity of R6G molecules, thereby significantly improving the detection sensitivity of the substrate. In Figure 8c, the spectral data of the characteristic peak of R6G molecules at 612 cm^{-1} at different concentrations are selected, and the concentration and Raman peak intensity are logarithmically transformed and linearly fitted. It can be seen that there is a good linear relationship between the logarithms of the concentration and intensity of R6G, with the coefficient of determination R^2 = 0.986, which is close to 1, further proving that the AuNRs@AAO substrate can be used as a SERS detection substrate.

Besides sensitivity, the uniformity of the substrate is also an important factor for evaluating the substrate. We randomly selected 10 locations on the substrate where R6G molecules were adsorbed at a concentration of 10^{-6} M for Raman signal testing, as illustrated in Figure 8d. The RSD of the Raman peak at 612 cm^{-1} was 4.3%, and the Raman peak of R6G did not shift. The Raman spectral intensity collected from the 10 randomly sampled points is detailed in Figure S4a, indicating that the AuNRs@AAO substrate has good uniformity.

To investigate the potential applications of the prepared substrate, we examined the Raman spectra of different concentrations of CV molecules (10^{-6}–10^{-12} M) on it. This testing was conducted using a 532 nm laser excitation, with the power of 2.5 mW and an integration time of 5 s. As illustrated in Figure 9a, the substrate demonstrates excellent sensitivity, and several characteristic peaks are clearly visible. Figure 9b demonstrates the enlarged Raman spectra for CV concentrations of 10^{-11} and 10^{-12} M in Figure 9a. Figure 9c displays the results of a linear fit of the logarithm of Raman signal against the molecular concentration located at the CV typical characteristic peak 1619 cm^{-1}, yielding a coefficient of determination of R^2 = 0.977. Additionally, Figure S4b features a waterfall plot of the intensity of the Raman signal from 10 randomly selected points on the substrate. Figure 9d shows the histogram of 10 randomly selected points at 1619 cm^{-1}, with a relative standard deviation RSD = 3.18%, indicating that the substrate exhibits good homogeneity.

APM is a noncarbohydrate artificial sweetener. The Joint Expert Committee on Food Additives, established by the Food and Agriculture Organization of the United Nations and the World Health Organization, has established a recommended daily intake of APM at 40 mg/kg. For an adult weighing 70 kg, the maximum permissible daily intake is 2800 mg.[44−47] SERS detection was conducted by immersing the substrate in aspartame solutions at concentrations of 0.5, 0.25, 0.125, 0.0625, 0.0313, 0.0156, and 0.0078 g/L. The SERS measurements were performed using a laser with a wavelength of 785 nm, an excitation time of 10 s, and excitation power of 4 mW. The Raman spectra are depicted in Figure 10, which reveals the characteristic Raman peaks of APM molecules at 746, 852, 934, 1003, and 1449 cm^{-1}. The detection limit was 7.8 mg/L, which

https://doi.org/10.1021/acsomega.5c00417
ACS Omega 2025, 10, 18764−18774

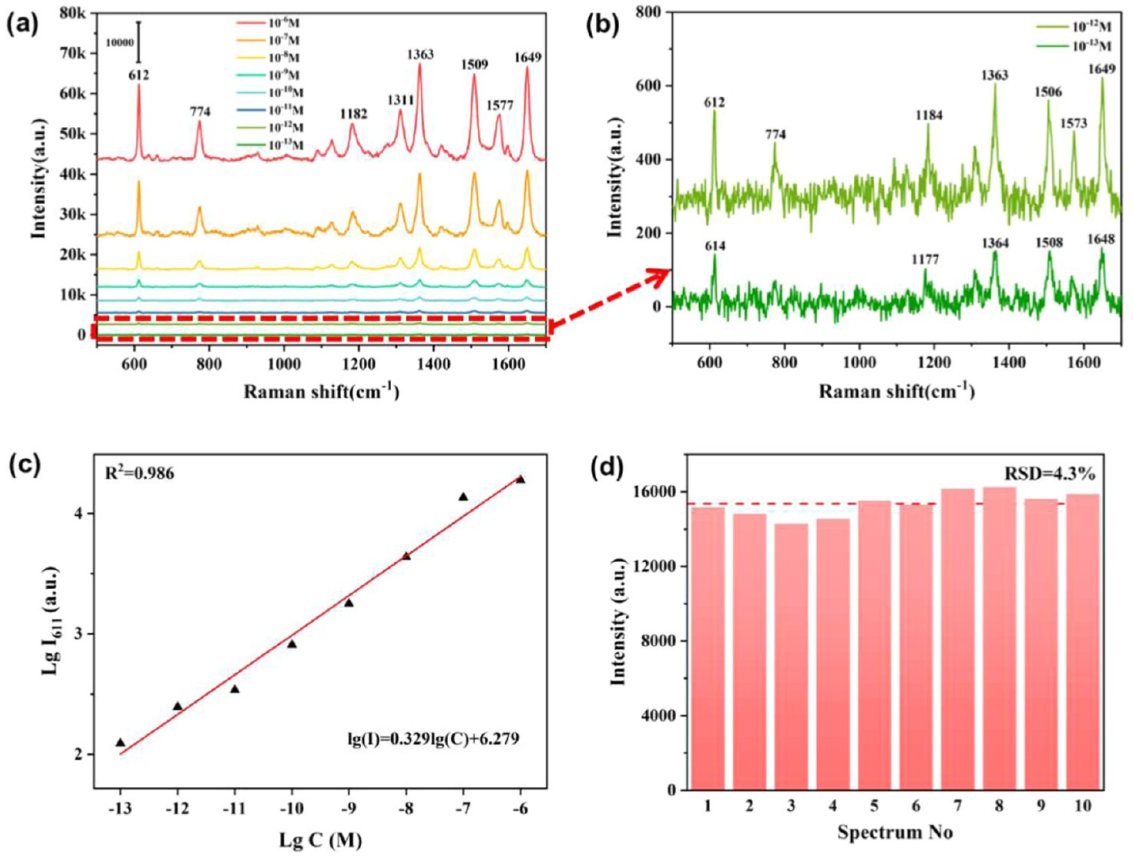

Figure 8. (a) Raman spectra of R6G molecules at different concentrations tested on the AuNRs@AAO substrate, with a detection limit of 10^{-13} M. (b) The enlarged Raman spectra for R6G concentration of 10^{-12} and 10^{-13} M in Figure (a). (c) The linear fitting graph between the logarithm of Raman intensity of the characteristic peaks and different concentrations of R6G molecules at 612 cm^{-1}. (d) Raman intensity histogram of 10 random points located at 612 cm^{-1} at a R6G concentration of 10^{-6} M.

is far below the established standards for additive limits. It suggests that the substrate exhibits a high level of detection sensitivity.

The fabrication of highly SERS-active substrates is fundamental to SERS research, and one of the requirements is their chemical and temporal stability. Taking the substrate adsorbed with 10^{-6} M R6G molecules as an example, the Raman spectral signal changes of R6G molecules adsorbed on the substrate surface after 30 days of placement were analyzed, as shown in Figure 11a. It was observed that the Raman signal intensity of R6G molecules would decrease to a certain extent over time. Specifically, Figure 11b presents the intensity of the characteristic peaks of R6G at 612, 774, 1363, 1508 and 1649 cm^{-1}. Notably, after 30 days of exposure to air, the Raman signals of R6G molecules remain detectable. Compared with the freshly prepared SERS substrate, the loss of Raman signal intensity at 612 cm^{-1} was less than 40%, and the intensity of Raman signal at other peaks decreased by approximately 50%.

In analytical chemistry applications, the analytical enhancement factor (AEF) is frequently employed to assess the enhancement capability of a substrate. AEF is a specific form of the enhancement factor (EF) and is particularly useful for quantifying the analytical signal enhancement. The following formula is commonly used to calculate the AEF:[48−50]

$$\mathrm{AEF} = \frac{I_{\mathrm{SERS}}/I_{\mathrm{Ref}}}{C_{\mathrm{SERS}}/C_{\mathrm{Ref}}} \quad (1)$$

where C_{SERS} and C_{Ref} are the concentrations of R6G on the AuNRs@AAO substrate (10^{-13} M) and reference substrate (10^{-3} M), respectively. I_{SERS} and I_{Ref} are the Raman signal intensity of R6G adsorbed on the substrate surface and the reference substrate. The Raman peak of the R6G molecule at 612 cm^{-1} was selected for calculation. Based on the spectral data, EF can be calculated to be 1.02×10^9. Similarly, the AEF values of CV and APM were 3.59×10^9 and 1.5×10^4. The concentration of adsorbed CV in the blank sample is 10^{-3} M, and the mass concentration of APM is 5 g/L. The SERS spectra of the blank samples are provided in the Figures S3b,c.

The finite element method (FEM) was employed to simulate the distribution of the local electromagnetic field of the substrate in the $x-y$ plane. The excitation light wavelength was set to 532 nm, and the incident light was directed perpendicularly to the substrate surface along the $-z$ axis. Based on the SEM images of the substrate, the AAO pore diameter was established at 90 nm, the pore depth was 90 nm, the length of the AuNRs was 80 nm, and the rod diameter was 16 nm in the simulation. The AuNRs were either randomly distributed within the pores in a "shoulder-to-shoulder" arrangement or scattered at the top. In the electric field distribution diagram, the electric field intensity can be precisely determined through the color exhibited therein. Precisely, as portrayed in Figure 12, a color of greater depth (or a red hue of higher intensity) precisely reflects a more significant enhancement of the local electric field. As illustrated in Figure 12a, when the rods are closely aligned horizontally within the pores, the electromagnetic "hot spots" are primarily located at

https://doi.org/10.1021/acsomega.5c00417
ACS Omega 2025, 10, 18764−18774

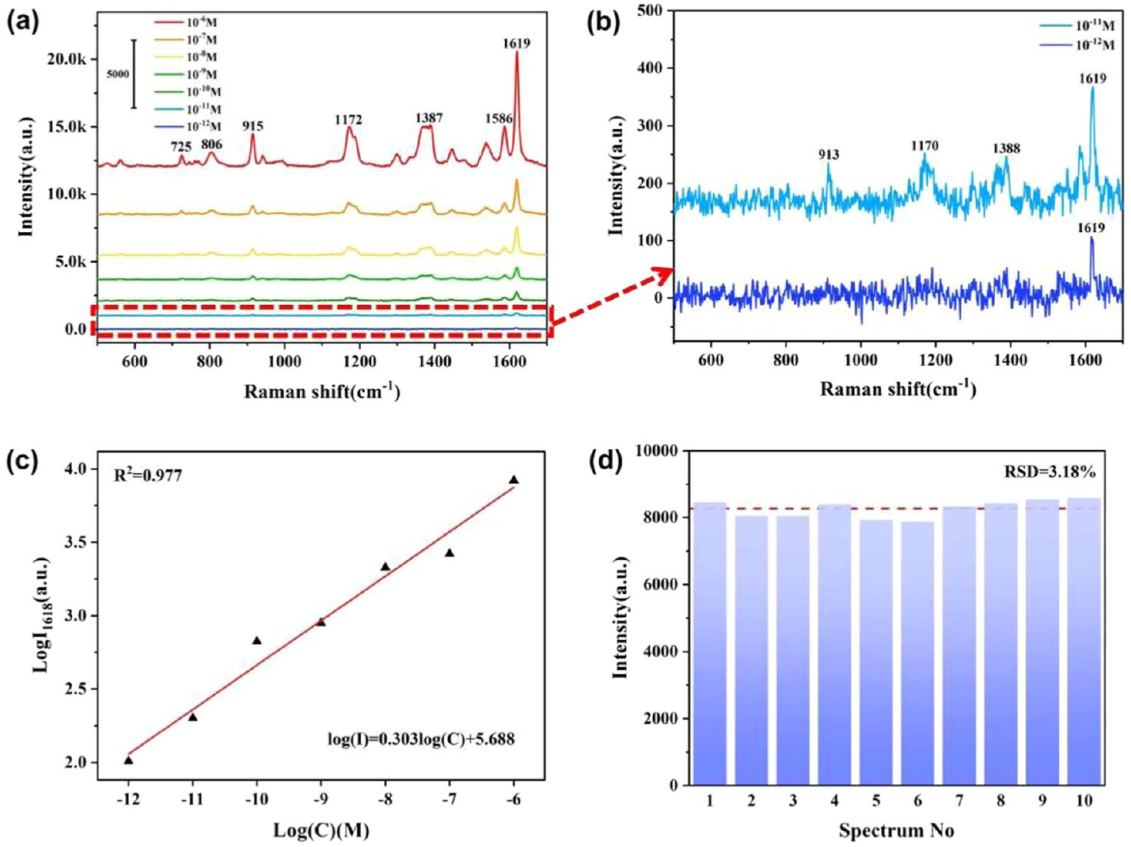

Figure 9. (a) SERS spectra of CV molecules at different concentrations on the AuNRs@AAO substrate. (b) The enlarged Raman spectra of CV concentrations of 10^{-11} and 10^{-12} M in Figure (a). (c) The fitting graph illustrating the relationship between the logarithm of Raman signal intensity of the characteristic peak and different concentrations of CV molecules at 1619 cm^{-1}. (d) A histogram of 10 randomly selected points on the surface at 1619 cm^{-1}, with a CV concentration of 10^{-6} M.

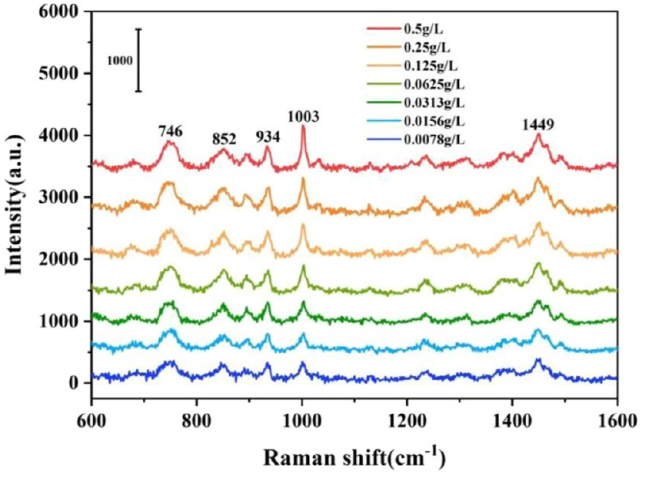

Figure 10. Comparative analysis of the concentration gradient signals of APM molecules tested on AuNRs@AAO substrate.

the ends of the rods. Figure 12b shows that when the particles are inclined within the pores and arranged in a dispersed manner at the top, the "hot spots" are mainly concentrated at the upper portions of the rods. Figure 12c presents a scenario in which more particles occupy the pores, with the majority of AuNRs positioned vertically along the pore walls, while a minority of AuNRs are scattered at various angles within the pores. In this case, the electromagnetic "hot spots" remain concentrated at the tops of the rods. However, a resonance coupling effect occurs in the narrow gaps between the rods, significantly enhancing the intensity of the Raman scattering signal.

3. CONCLUSIONS

In this paper, we successfully assembled AuNRs into AAO pores using a three-phase system to prepare a relatively ordered supersensitive SERS detection substrate. We investigated the influence of AAO pore size and AuNRs LSPR position on the substrate's performance. The results indicated that the optimal conditions for substrate assembly are an oxidation voltage of 45 V and a pore expansion time of 45 min, with AuNRs LSPR peak of about 800 nm. R6G, CV, and APM molecules can be detected experimentally at concentrations as low as 10^{-13}, 10^{-12} M and 7.8 mg/L, respectively. And the EF values were calculated to be 1.02×10^9, 3.59×10^9, and 1.5×10^4, suggesting that the developed substrate exhibits commendable reproducibility and uniformity. Additionally, the ordered arrangement and interstitial structure of AuNRs provide opportunities for applications in fields such as photothermal therapy. Therefore, this substrate has a promising application in the fields of environmental detection, food detection and photothermal therapy.

4. EXPERIMENTAL SECTION

The AAO template was made using a two-step anodization process. In the first step, the cleaned aluminum substrate was immersed in an electrolyte solution and a certain voltage was applied for anodization to form an initial oxide layer. In the second step, the anodization process was continued at the same

https://doi.org/10.1021/acsomega.5c00417
ACS Omega 2025, 10, 18764−18774

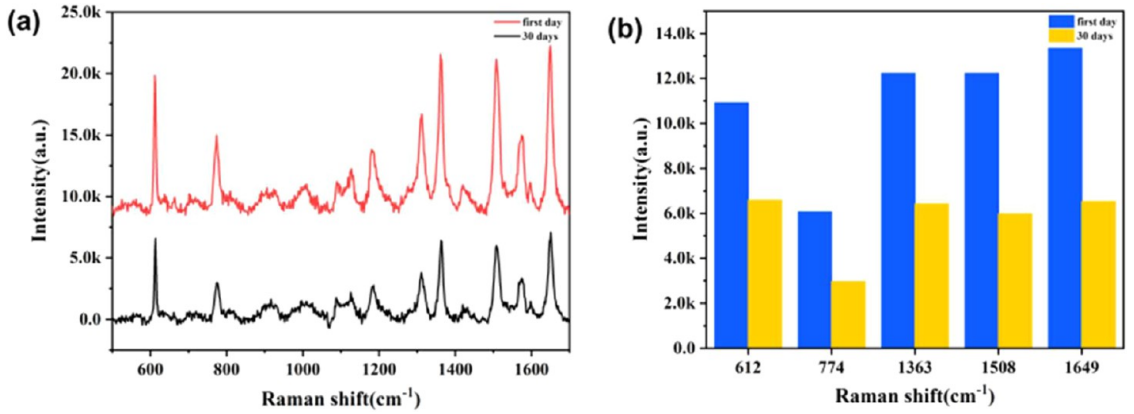

Figure 11. (a) Stability detection and comparative analysis of the substrate. (b) Comparison of the Raman signal intensity at the characteristic peaks at 612, 774, 1363, 1508 and 1649 cm^{-1}.

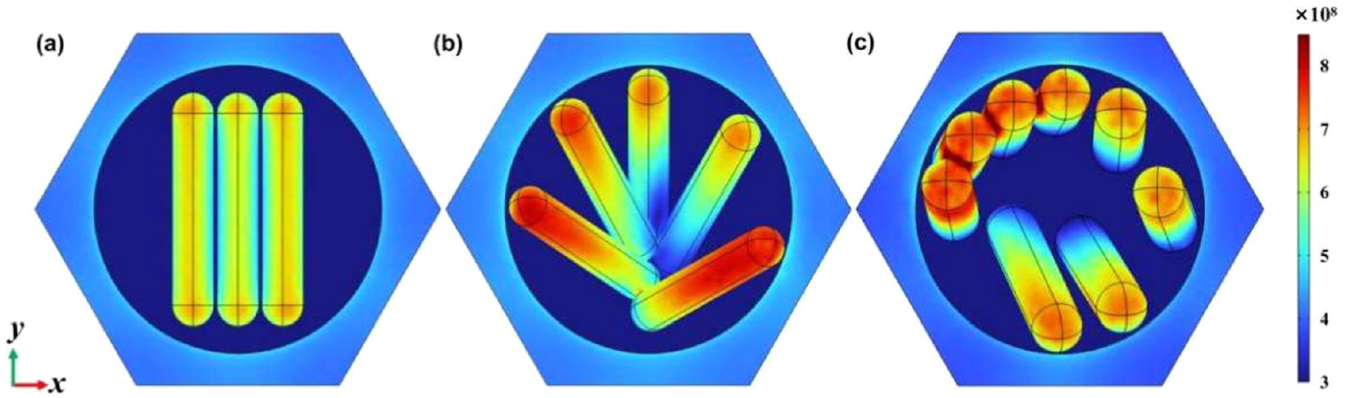

Figure 12. (a−c) COMSOL simulation of different distribution states of different numbers of AuNRs in the hole: local electric field distribution of the substrate in the $x-y$ plane.

voltage. The pore size of the AAO template was systematically controlled by adjusting the oxidation voltage. Finally, the template was immersed in an acidic solution for a period of time to achieve pore size enlargement.

AuNRs were synthesized by the seed-mediated growth method. Initially, gold seeds with a small diameter were prepared in a solution containing $HAuCl_4$ and a reducing agent. Then, a growth solution composed of $HAuCl_4$, $AgNO_3$, and a reducing agent was prepared. The aspect ratio of the AuNRs was controlled by adjusting the amount of $AgNO_3$ and the pH value of the solution. Subsequently, the prepared seed solution was added to the growth solution, and the reaction time was strictly controlled. Finally, a colloidal solution of AuNRs was obtained by centrifugation and purification.

To fabricate the AuNRs@AAO composite substrate, a three-phase self-assembly technique was employed to assemble AuNRs into the pores of the AAO template. Detailed information regarding reagents, experimental conditions, and procedural steps is provided in the Supporting Information.

■ ASSOCIATED CONTENT

Supporting Information

The Supporting Information is available free of charge at https://pubs.acs.org/doi/10.1021/acsomega.5c00417.

Preparation procedure of the AAO template and the detection limits of AuNRs@AAO substrates are described here; vertical section of the naturally fractured AAO film and measures the average hole depth to be about 88 nm (Figure S1); absorption spectrum analysis of Au NRs solutions (Figure S2a,b, and d); SEM image of 880 nm AuNRs assembled on silicon wafer through three-phase assembly method (Figure S2c); Raman spectroscopic characterization images of various analytes adsorbed on blank AAO substrates (Figure S3); SERS signal of R6G and CV molecules deposited on the fabricated substrate (Figure S4) (PDF)

■ AUTHOR INFORMATION

Corresponding Authors

Jun Dong − *School of Electronic Engineering, Xi'an University of Posts and Telecommunications, Xi'an 710121, China;* orcid.org/0000-0001-7226-613X; Email: dongjun@xupt.edu.cn

Wei Gao − *School of Electronic Engineering, Xi'an University of Posts and Telecommunications, Xi'an 710121, China;* Email: gaowei@xupt.edu.cn

Authors

Ziqing Fang − *School of Electronic Engineering, Xi'an University of Posts and Telecommunications, Xi'an 710121, China*

Yimeng Fan − *School of Electronic Engineering, Xi'an University of Posts and Telecommunications, Xi'an 710121, China*

Chenlu Li − *School of Electronic Engineering, Xi'an University of Posts and Telecommunications, Xi'an 710121, China*

https://doi.org/10.1021/acsomega.5c00417
ACS Omega 2025, 10, 18764−18774

Qingyan Han − *School of Electronic Engineering, Xi'an University of Posts and Telecommunications, Xi'an 710121, China*
Chengyun Zhang − *School of Electronic Engineering, Xi'an University of Posts and Telecommunications, Xi'an 710121, China*
Lipeng Zhu − *School of Electronic Engineering, Xi'an University of Posts and Telecommunications, Xi'an 710121, China*
Xuewen Yan − *School of Electronic Engineering, Xi'an University of Posts and Telecommunications, Xi'an 710121, China*
Jianxia Qi − *School of Science, Xi'an University of Posts and Telecommunications, Xi'an 710121, China*

Complete contact information is available at: https://pubs.acs.org/10.1021/acsomega.5c00417

Notes

The authors declare no competing financial interest.

■ ACKNOWLEDGMENTS

This work was financially supported by The National Natural Science Foundation of China (12274341), the Shaanxi province Natural Science Foundation of China (2022JZ-05), and Innovation Funds of Graduate Programs of Xi'an University of Posts & Telecommunications (CXJJZL2023014).

■ REFERENCES

(1) Fleischmann, M.; Hendra, P. J.; McQuillan, A. J. Raman spectra of pyridine adsorbed at a silver electrode. *Chem. Phys. Lett.* **1974**, *26* (2), 163−166.
(2) Albrecht, M. G.; Creighton, J. A. Anomalously intense Raman spectra of pyridine at a silver electrode. *J. Am. Chem. Soc.* **1977**, *99* (15), 5215−5217.
(3) Kruszewski, S. Dependence of SERS signal on surface roughness. *Surf. Interface Anal.* **1994**, *21* (12), 830−838.
(4) Doering, W. E.; Piotti, M. E.; Natan, M. J.; Freeman, R. G. SERS as a foundation for nanoscale, optically detected biological labels. *Adv. Mater.* **2007**, *19* (20), 3100−3108.
(5) Dong, J.; Zhou, W. T.; Yang, C. Y.; Wu, H. R.; Han, Q. Y.; Zhang, C. Y.; Gao, W.; Yan, X. W.; Sun, M. T. Preparation of a Three-Dimensional Composite Structure Based on a Periodic Au@Ag Core−Shell Nanocube with Ultrasensitive Surface-Enhanced Raman Scattering for Rapid Detection. *ACS Appl. Mater. Interfaces* **2023**, *15* (23), 28840−28848.
(6) Samanta, A.; Maiti, K. K.; Soh, K.-S.; Liao, X.; Vendrell, M.; Dinish, U. S.; Yun, S.-W.; Bhuvaneswari, R.; Kim, H.; Rautela, S.; et al. Ultrasensitive near-infrared Raman reporters for SERS-based in vivo cancer detection. *Angew. Chem.* **2011**, *50* (27), 6089−6092.
(7) Guerrini, L.; Krpetić, Ž.; van Lierop, D.; Alvarez-Puebla, R. A.; Graham, D. Direct Surface-Enhanced Raman Scattering Analysis of DNA Duplexes. *Angew. Chem.* **2015**, *127* (4), 1160−1164.
(8) Andreou, C.; Neuschmelting, V.; Tschaharganeh, D.-F.; Huang, C.-H.; Oseledchyk, A.; Iacono, P.; Karabeber, H.; Colen, R. R.; Mannelli, L.; Lowe, S. W.; Kircher, M. F. Imaging of liver tumors using surface-enhanced Raman scattering nanoparticles. *ACS Nano* **2016**, *10* (5), 5015−5026.
(9) Zhao, X.; Dong, J.; Cao, E.; Han, Q. Y.; Gao, W.; Wang, Y. K.; Qi, J. X.; Sun, M. T. Plasmon-exciton coupling by hybrids between graphene and Au nanorods vertical array for sensor. *Appl. Mater. Today* **2019**, *14*, 166−174.
(10) Song, C. Y.; Yang, Y. J.; Yang, B. Y.; Sun, Y. Z.; Zhao, Y. P.; Wang, L. H. An ultrasensitive SERS sensor for simultaneous detection of multiple cancer-related miRNAs. *Nanoscale* **2016**, *8* (39), 17365−17373.
(11) Betz, J. F.; Wei, W. Y.; Cheng, Y.; White, I. M.; Rubloff, G. W. Simple SERS substrates, powerful, portable, and full of potential. *Phys. Chem. Chem. Phys.* **2014**, *16* (6), 2224−2239.
(12) Zhang, Q.; Lee, Y. H.; Phang, I. Y.; Lee, C. K.; Ling, X. Y. Hierarchical 3D SERS substrates fabricated by integrating photolithographic microstructures and self-assembly of silver nanoparticles. *Small* **2014**, *10* (13), 2703−2711.
(13) Wang, Y.; Yu, Y.; Liu, Y.; Yang, S. Template-confined site-specific electrodeposition of nanoparticle cluster-in-bowl arrays as surface enhanced Raman spectroscopy substrates. *ACS Sens.* **2018**, *3* (11), 2343−2350.
(14) Fu, Z. W.; Shen, Z. D.; Fan, Q. Z.; Hao, S. X.; Wang, Y.; Liu, X. Q.; Tong, X. X.; Kong, X. M.; Yang, Z. X. Preparation of multi-functional magnetic-plasmonic nanocomposite for adsorption and detection of thiram using SERS. *J. Hazard. Mater.* **2020**, *392*, No. 122356.
(15) Yu, Z.; Jiang, L.; Liu, R.; Zhao, W.; Yang, Z.; Zhang, J.; Jin, S. Versatile self-assembled MXene-Au nanocomposites for SERS detection of bacteria, antibacterial and photothermal sterilization. *Chem. Eng. J.* **2021**, *426*, No. 131914.
(16) Lin, D. D.; Wu, Z. L.; Li, S. J.; Zhao, W. Q.; Ma, C. J.; Wang, J.; Jiang, Z. M.; Zhong, Z. Y.; Zheng, Y. B.; Yang, X. J. Large-area Au-nanoparticle-functionalized Si nanorod arrays for spatially uniform surface-enhanced Raman spectroscopy. *ACS Nano* **2017**, *11* (2), 1478−1487.
(17) Xu, W.; Meng, G. W.; Huang, Q.; Hu, X. Y.; Huang, Z. L.; Tang, H. B.; Zhang, J. X. Large-scale uniform Ag-NW tip array with enriched sub-10-nm gaps as SERS substrate for rapid determination of trace PCB77. *Appl. Surf. Sci.* **2013**, *271*, 125−130.
(18) Daniel, S.; Matikainen, A.; Turunen, J.; Vahimaa, P.; Nuutinen, T. Uniform distribution of Ag particles upon imprinted polymer grating for Raman signal enhancement. *J. Colloid Interface Sci.* **2015**, *437*, 119−123.
(19) Xu, W.; Okamoto, T.; Li, A.; Wang, J.; Haraguchi, M. Preparation of large-area controllable patterned silver nanocrystals for high sensitive and stable surface-enhanced Raman spectroscopy. *Chem. Res. Chin. Univ.* **2016**, *32*, 428−432.
(20) Yi, Z.; Ye, X.; Luo, J. S.; Kang, X. L.; Yi, Y. G.; Yi, Y.; Huang, J.; Jiang, X. D.; Tang, Y. J. Ordered hexagonal nanoplasmonic au nanoparticle arrays, AAO-assisted thermal treatment synthesis and application as surface-enhanced Raman scattering substrates. *Plasmonics* **2017**, *12*, 2013−2020.
(21) Kang, M. Y.; Zhang, X. Y.; Liu, L. W.; Zhou, Q. W.; Jin, M. L.; Zhou, G. F.; Gao, X. S.; Lu, X. B.; Zhang, Z.; Liu, J. M. High-density ordered Ag@Al_2O_3 nanobowl arrays in applications of surface-enhanced Raman spectroscopy. *Nanotechnology* **2016**, *27* (16), No. 165304.
(22) Md Jani, A. M.; Losic, D.; Voelcker, N. H. Nanoporous anodic aluminium oxide, Advances in surface engineering and emerging applications. *Prog. Mater. Sci.* **2013**, *58* (5), 636−704.
(23) Wehrspohn, R. B. Ordered Porous Nanostructures and Applications. In *Nanostructure Science and Technology*; Springer: New York, 2005.
(24) Ruiz-Clavijo, A.; Caballero-Calero, O.; Martín-González, M. Revisiting anodic alumina templates, From fabrication to applications. *Nanoscale* **2021**, *13* (4), 2227−2265.
(25) Steinhart, M.; Wendorff, J. H.; Greiner, A.; Wehrspohn, R. B.; Nielsch, K.; Schilling, J.; Choi, J.; Gösele, U. Polymer nanotubes by wetting of ordered porous templates. *Science* **2002**, *296* (5575), 1997.
(26) Jans, H.; Huo, Q. Gold nanoparticle-enabled biological and chemical detection and analysis. *Chem. Soc. Rev.* **2012**, *41* (7), 2849−2866.
(27) Tezcan, T.; Boyaci, I. H. A new and facile route to prepare gold nanoparticle clusters on anodic aluminium oxide as a SERS substrate. *Talanta* **2021**, *232*, No. 122426.
(28) Huang, Z. L.; Meng, G. W.; Huang, Q.; Chen, B.; Zhu, C. H.; Zhang, Z. Large-area Ag nanorod array substrates for SERS, AAO template-assisted fabrication, functionalization, and application in detection PCBs. *J. Raman Spectrosc.* **2013**, *44* (2), 240−246.

(29) Liao, Q.; Mu, C.; Xu, D. S.; Ai, X. C.; Yao, J. N.; Zhang, J. P. Gold nanorod arrays with good reproducibility for high-performance surface-enhanced Raman scattering. *Langmuir* **2009**, *25* (8), 4708−4714.
(30) Bui, T. L.; Ho, N. T.; Ho, X. V. T. T.; Ngo, D. N.; Lim, S. H.; Son, S. J.; Noh, S. M.; Joo, S. W. Plasmonic nanorod array for effective photothermal therapy in hyperthermia. *Chem. Commun.* **2021**, *57* (71), 8961−8964.
(31) Lê, Q. T.; Ly, N. H.; Kim, M. K.; Lim, S. H.; Son, S. J.; Zoh, K. D.; Joo, S. W. Nanostructured Raman substrates for the sensitive detection of submicrometer-sized plastic pollutants in water. *J. Hazard. Mater.* **2021**, *402*, No. 123499.
(32) Dong, J.; Li, C. L.; Wang, Y.; Fan, Y. M.; Han, Q. Y.; Gao, W.; Wang, Y. K.; Ren, K. L.; Qi, J. X.; He, E. J. Fabrication of complexed nanostructure using AAO template for ultrasensitive SERS detection. *Spectrochim. Acta, Part A* **2024**, *312*, No. 124044.
(33) Wang, K.; Jin, S. M.; Xu, J. P.; Liang, R. J.; Shezad, K.; Xue, Z. G.; Xie, X. L.; Lee, E.; Zhu, J. T. Electric-field-assisted assembly of polymer-tethered gold nanorods in cylindrical nanopores. *ACS Nano* **2016**, *10* (5), 4954−4960.
(34) Song, Y. J.; Wang, Y.; Li, B. B.; Fernandes, C.; Ruda, H. E. Interface interaction induced ultra-dense nanoparticles assemblies. *Nanoscale* **2013**, *5* (15), 6779−6789.
(35) Jain, P. K.; Lee, K. S.; El-Sayed, I. H.; El-Sayed, M. A. Calculated absorption and scattering properties of gold nanoparticles of different size, shape, and composition, applications in biological imaging and biomedicine. *J. Phys. Chem. B* **2006**, *110* (14), 7238−7248.
(36) Fang, Y.; Seong, N. H.; Dlott, D. D. Measurement of the distribution of site enhancements in surface-enhanced Raman scattering. *Science* **2008**, *321* (5887), 388−392.
(37) Lin, X.; Fang, G. Q.; Liu, Y. L.; He, Y. Y.; Wang, L.; Dong, B. Marangoni effect-driven transfer and compression at three-phase interfaces for highly reproducible nanoparticle monolayers. *J. Phys. Chem. Lett.* **2020**, *11* (9), 3573−3581.
(38) Lee, S. M.; Nam, D. H.; Lee, D.; Lim, S. H.; Son, S. J.; Lee, S. Gold nanoparticles deposited on a conical anodic aluminum oxide substrate for improved surface-enhanced Raman scattering. *ACS Appl. Nano Mater.* **2021**, *4* (12), 12905−12912.
(39) Redón, R.; Vázquez-Olmos, A.; Mata-Zamora, M. E.; Ordóñez-Medrano, A.; Rivera-Torres, F.; Saniger, J. M. Contact angle studies on anodic porous alumina. *J. Colloid Interface Sci.* **2005**, *287* (2), 664−670.
(40) Toma, H. E.; Zamarion, V. M.; Toma, S. H.; Araki, K. The coordination chemistry at gold nanoparticles. *J. Braz. Chem. Soc.* **2010**, *21* (7), 1158−1176.
(41) Kuemin, C.; Stutz, R.; Spencer, N. D.; Wolf, H. Precise placement of gold nanorods by capillary assembly. *Langmuir* **2011**, *27* (10), 6305−6310.
(42) Dieringer, J. A.; Wustholz, K. L.; Masiello, D. J.; Camden, J. P.; Kleinman, S. L.; Schatz, G. C.; Van Duyne, R. P. Surface-enhanced Raman excitation spectroscopy of a single rhodamine 6G molecule. *J. Am. Chem. Soc.* **2009**, *131* (2), 849−854.
(43) Mijangos, C.; Hernández, R.; Martín, J. A review on the progress of polymer nanostructures with modulated morphologies and properties, using nanoporous AAO templates. *Prog. Polym. Sci.* **2016**, *54-55*, 148−182.
(44) *Evaluation of Certain Food Additives, Ninety-Sixth Report of the Joint FAO/WHO Expert Committee on Food Additives*; World Health Organization, 2024.
(45) Anton, S. D.; Martin, C. K.; Han, H.; Coulon, S.; Cefalu, W. T.; Geiselman, P.; Williamson, D. A. Effects of stevia, aspartame, and sucrose on food intake, satiety, and postprandial glucose and insulin levels. *Appetite* **2010**, *55* (1), 37−43.
(46) *Aspartame Hazard and Risk Assessment Results Released.*; World Health Organization, 2023; Vol. *14*.
(47) Magnuson, B. A.; Burdock, G. A.; Doull, J.; Kroes, R. M.; Marsh, G. M.; Pariza, M. W.; Spencer, P. S.; Waddell, W. J.; Walker, R.; Williams, G. M. Aspartame, a safety evaluation based on current use levels, regulations, and toxicological and epidemiological studies. *Crit. Rev. Toxicol.* **2007**, *37* (8), 629−727.
(48) Le Ru, E. C.; Blackie, E.; Meyer, M.; Etchegoin, P. G. Surface enhanced Raman scattering enhancement factors, a comprehensive study. *J. Phys. Chem. C* **2007**, *111* (37), 13794−13803.
(49) Zhang, W. W.; Tian, Q. K.; Chen, Z. H.; Zhao, C. C.; Chai, H. S.; Wu, Q.; Li, W. G.; Chen, X. H.; Deng, Y. D.; Song, Y. J. Arrayed nanopore silver thin films for surface-enhanced Raman scattering. *RSC Adv.* **2020**, *10* (40), 23908−23915.
(50) Zhang, W.; Zhu, X.; Chen, Z.; Belotelov, V. I.; Song, Y. Silver nanopillar arrayed thin films with highly surface-enhanced Raman scattering for ultrasensitive detection. *ACS Omega* **2022**, *7* (29), 25726−25731.

https://doi.org/10.1021/acsomega.5c00417
ACS Omega 2025, 10, 18764−18774